# Solar sail optimal control with solar irradiance fluctuations

Andrea Caruso*, Giovanni Mengali, Alessandro A. Quarta, Lorenzo Niccolai

*Dipartimento di Ingegneria Civile e Industriale, University of Pisa, I-56122 Pisa, Italy*

**Abstract**

The optimization of a solar sail-based orbital transfer amounts to searching for the control law that minimizes the flight time. In this context, the optimal trajectory is usually determined assuming constant solar properties. However, the total solar irradiance undergoes both long-term (solar cycles) and short-term variations, and recent analyses have shown that this may have an impact on solar sailing for missions requiring an accurate thrust modulation. In this regard, the paper discusses a strategy to overcome such an issue by suitably adjusting the thrust vector in order to track a reference, optimal, transfer trajectory. In particular, the sail propulsive acceleration magnitude is modified by means of a set of electrochromic material panels, which change their optical properties on application of a suitable electric voltage. The proposed control law is validated with a set of numerical simulations that involve a classical Earth-Mars, orbit-to-orbit, heliocentric transfer.

*Keywords:* Solar sail, solar irradiance fluctuations, electrochromic material panels

**Nomenclature**

| | | |
|---|---|---|
| $A$ | = | sail area, [$\mathrm{m}^2$] |
| $\boldsymbol{a}$ | = | propulsive acceleration vector, [$\mathrm{mm/s}^2$] |
| $a_c$ | = | characteristic acceleration, [$\mathrm{mm/s}^2$] |
| $a_r$ | = | radial component of propulsive acceleration, [$\mathrm{mm/s}^2$] |
| $a_t$ | = | transverse component of propulsive acceleration, [$\mathrm{mm/s}^2$] |
| $\{B_f,\, B_b\}$ | = | sail film front and back non-Lambertian coefficients |
| $\{b_1, b_2, b_3\}$ | = | sail force coefficients |
| $c$ | = | speed of light, [km/s] |
| $f$ | = | fraction of specularly-reflective surface |
| $\{\hat{\boldsymbol{\imath}}_R, \hat{\boldsymbol{\imath}}_T, \hat{\boldsymbol{\imath}}_N\}$ | = | unit vectors of RTN reference frame |
| $K_i$ | = | auxiliary parameters ($i = 1, \ldots, 7$), see Eqs. (22) |
| $m$ | = | spacecraft total mass, [kg] |
| $\hat{\boldsymbol{n}}$ | = | normal unit vector |
| $\boldsymbol{r}$ | = | spacecraft position vector, [au] |
| $\hat{\boldsymbol{r}}$ | = | spacecraft position unit vector |
| $r$ | = | Sun-spacecraft distance, [au] |
| $S$ | = | spacecraft center-of-mass |
| $s$ | = | fraction of specularly-reflected photons |
| $\hat{\boldsymbol{t}}$ | = | transverse unit vector |
| $t$ | = | time, [days] |

*Corresponding author

*Email addresses:* andrea.caruso@ing.unipi.it (Andrea Caruso), g.mengali@ing.unipi.it (Giovanni Mengali), a.quarta@ing.unipi.it (Alessandro A. Quarta), lorenzo.niccolai@ing.unipi.it (Lorenzo Niccolai)

Published in Advances in Space Research, Vol. 67, No. 9, May 2021, pp. 2776–2783. doi: https://doi.org/10.1016/j.asr.2020.05.037

| | | |
|---|---|---|
| $t_f$ | = | flight time, [days] |
| $\boldsymbol{v}$ | = | velocity vector, [km/s] |
| $W$ | = | total solar irradiance, [W/m$^2$] |
| $\alpha$ | = | sail cone angle, [deg] |
| $\Delta t_c$ | = | solar cycle duration, [years] |
| $\Delta W_\oplus$ | = | peak-to-peak amplitude of $W_\oplus$, [W/m$^2$] |
| $\delta$ | = | sail clock angle, [deg] |
| $\{\epsilon_f, \epsilon_b\}$ | = | sail film front and back emissivities |
| $\mu_\odot$ | = | Sun's gravitational parameter, [km$^3$/s$^2$] |
| $\mu_{W_\oplus}$ | = | mean value of $W_\oplus$, [W/m$^2$] |
| $\rho$ | = | sail film reflection coefficient |
| $\sigma_{W_\oplus}$ | = | standard deviation of $W_\oplus$, [W/m$^2$] |

*Subscripts*

| | | |
|---|---|---|
| $\oplus$ | = | at 1 au from the Sun |
| EMP | = | electrochromic material panels |
| tot | = | total |
| $s$ | = | reflective film |

*Superscripts*

| | | |
|---|---|---|
| $\cdot$ | = | time derivative |
| $-$ | = | constant value |
| $\sim$ | = | dimensionless |
| min | = | minimum value |
| off | = | relative to diffuse reflection |
| on | = | relative to specular reflection |
| ref | = | reference value |

## 1. Introduction

The design of a heliocentric orbit-to-orbit trajectory of a solar sail-based spacecraft is usually carried out by looking for the control law that minimizes the total flight time [25, 10, 12]. In such an optimization problem, the total solar irradiance (TSI), which is exploited to generate thrust, is customarily assumed to be constant. However, the TSI is subjected to time fluctuations related to the well known 11-year solar cycles [24, 9], upon which are superimposed short-term (small) random variations [16, 8]. Refined analyses in this regard [26, 27] have shown that TSI fluctuations may have a non-negligible effect on the solar sail transfer trajectory [5]. Therefore, a control strategy capable of steering the spacecraft toward the final target state should be considered in a second phase of trajectory design.

This paper proposes a possible solution to this problem, based on the use of electrochromic material panels (EMPs), which are able to change their optical properties on application of a suitable electric voltage [20]. In particular, the state of EMPs can be switched between high (power-on state) and diffuse (power-off state) reflection. Recent studies have analyzed the performance of EMP as an attitude control device [21], and the whole concept has been successfully tested on the pioneering IKAROS mission [11, 15, 14]. However, because EMPs have also been proposed as a mean to modulate the propulsive acceleration magnitude [1, 19] especially in a case of high area-to-mass ratio [22], the use of an electrochromic film is exploited in this study as a possible way to counteract the TSI fluctuations.

More precisely, an optimal reference trajectory is first generated by considering constant solar properties and by using a classical approach to transfer optimization [18, 23, 3, 6]. The TSI temporal variations are then simulated according to the recent model proposed by [5], which describes the TSI fluctuations using

a Gaussian distribution superimposed to a sinusoidal function to take into account both the 11-year solar cycles and the short-term random fluctuations. A more accurate description of the TSI temporal variations should resort to a time series analysis [26, 7], which would require a large amount of data. However, the accuracy of the simplified model may be verified by comparing its outputs with the recent data from the SORCE mission, as done by [5], and with the distribution of TSI daily means for cycles 21-22-23 reported by [28]. The latter has a standard deviation equal to $0.56\,\mathrm{W/m^2}$, a skewness equal to 0.118, and a kurtosis equal to 4.19, whereas [5] use a Gaussian distribution (skewness equal to 0, and kurtosis equal to 3) with a standard deviation of $2.35\,\mathrm{W/m^2}$, which is superimposed to a sinusoidal function to model the solar cycles. Therefore, it may be concluded that the results obtained with a Gaussian model are conservative and useful for a preliminary study. To simplify the analysis and get some preliminary information about orbit-transfer attitude control, we will make a number of approximations as a first step to deal with the non-constant TSI problem, with special attention to TSI fluctuations. In particular, the dependence of the optical properties on some features of the reflecting surface (including its roughness) and on light polarization [29] are not considered in the following discussion. The same remark applies to other sources of uncertainty, such as orbital determination and control of execution errors.

Assuming the spacecraft to be capable of measuring, at each time, the local value of TSI and the sail attitude angles, it is possible to calculate the fraction of EMPs that must change their state so that the spacecraft may track the optimal reference trajectory. In this context, the optimal control law consists in a reference control history (obtained considering the total solar irradiance as a constant), upon which is superimposed a sort of compensation control law, which is obtained by varying the reflectivity of the electrochromic panels in such a way as to counteract the actual fluctuations of the solar irradiance.

This paper is organized as follows. Next section shows the control strategy used to counteract the effects of TSI fluctuations. Then, the proposed method is applied to an example mission scenario consistent with a classical Earth-Mars, orbit-to-orbit, heliocentric transfer. Finally, last section illustrates the main outcomes and conclusions.

## 2. Mathematical model

Consider a heliocentric orbit-to-orbit transfer of a solar sail-based spacecraft $S$ of which the dynamics is described by the equations of motion

$$\dot{\boldsymbol{r}} = \boldsymbol{v} \quad , \quad \dot{\boldsymbol{v}} = -\frac{\mu_\odot}{r^3}\boldsymbol{r} + \boldsymbol{a} \tag{1}$$

where $\boldsymbol{r}$ (or $\boldsymbol{v}$) is the spacecraft position (or velocity) vector, $r = \|\boldsymbol{r}\|$ is the Sun-spacecraft distance, $\mu_\odot$ is the Sun's gravitational parameter, and $\boldsymbol{a}$ is the sail propulsive acceleration vector. Assuming a flat solar sail, the vector $\boldsymbol{a}$ can be written using an optical force model as [17]

$$\boldsymbol{a} = \frac{W_\oplus\, A_{\mathrm{tot}}}{c\, m}\left(\frac{r_\oplus}{r}\right)^2 (\hat{\boldsymbol{n}}\cdot\hat{\boldsymbol{r}})\Big[b_1\,\hat{\boldsymbol{r}} + (b_2\,\hat{\boldsymbol{n}}\cdot\hat{\boldsymbol{r}} + b_3)\,\hat{\boldsymbol{n}}\Big] \tag{2}$$

where $r_\oplus \triangleq 1\,\mathrm{au}$ is a reference distance, $c$ is the speed of light in a vacuum, $W_\oplus$ is the TSI measured at a distance $r = r_\oplus$ from the Sun, $A_{\mathrm{tot}}$ is the sail total reflective area, $m$ is the total spacecraft mass, $\hat{\boldsymbol{r}} \triangleq \boldsymbol{r}/r$ is the Sun-spacecraft unit vector, $\hat{\boldsymbol{n}}$ is the unit vector normal to the sail nominal plane in the direction opposite to the Sun, and $\{b_1, b_2, b_3\}$ are the sail force dimensionless coefficients. The values of $\{b_1, b_2, b_3\}$ depend on the thermo-optical properties of the sail film through the equations [18]

$$b_1 = 1 - \rho s \tag{3}$$

$$b_2 = 2\rho s \tag{4}$$

$$b_3 = B_f\rho(1-s) + (1-\rho)\frac{\epsilon_f B_f - \epsilon_b B_b}{\epsilon_f + \epsilon_b} \tag{5}$$

where $\rho$ is the reflection coefficient, $s$ is the fraction of photons that are specularly reflected, $B_f$ (or $B_b$) is the non-Lambertian coefficient of the front (or back) sail film, and $\epsilon_f$ (or $\epsilon_b$) is the front (or back) sail film emissivity.

The normal unit vector $\hat{\boldsymbol{n}}$ is usually expressed in a radial-tangential-normal reference frame $\mathcal{T}_{\text{RTN}}(S; \hat{\boldsymbol{i}}_R, \hat{\boldsymbol{i}}_T, \hat{\boldsymbol{i}}_N)$, with unit vectors defined as

$$\hat{\boldsymbol{i}}_R \equiv \hat{\boldsymbol{r}} \quad , \quad \hat{\boldsymbol{i}}_N \triangleq \frac{\boldsymbol{r} \times \boldsymbol{v}}{\|\boldsymbol{r} \times \boldsymbol{v}\|} \quad , \quad \hat{\boldsymbol{i}}_T \triangleq \hat{\boldsymbol{i}}_N \times \hat{\boldsymbol{i}}_R \tag{6}$$

In particular, the expression of $\hat{\boldsymbol{n}}$ in $\mathcal{T}_{\text{RTN}}$ is

$$\hat{\boldsymbol{n}} = \cos\alpha\, \hat{\boldsymbol{i}}_R + \sin\alpha\, \cos\delta\, \hat{\boldsymbol{i}}_T + \sin\alpha\, \sin\delta\, \hat{\boldsymbol{i}}_N \tag{7}$$

where $\alpha \in [0, 90]$ deg is the cone angle, and $\delta \in [-180, 180)$ deg is the clock angle; see Fig. 1. Using Eqs. (2)

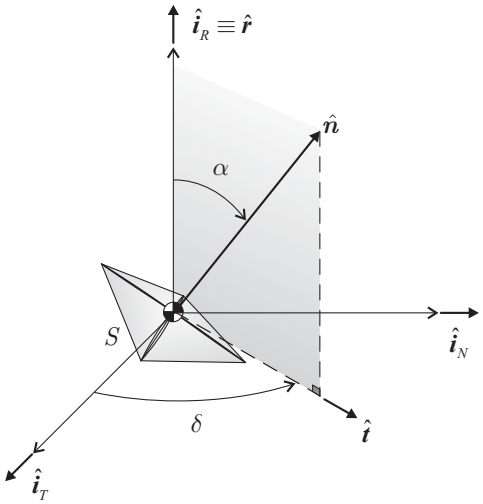


Figure 1: Orbital reference frame $\mathcal{T}_{\text{RTN}}$ and sail control angles $\{\alpha, \delta\}$.

and (7), the propulsive acceleration vector can be rewritten, more conveniently, as [17]

$$\boldsymbol{a} = a_r\, \hat{\boldsymbol{r}} + a_t\, \hat{\boldsymbol{t}} \tag{8}$$

where $\hat{\boldsymbol{t}}$ is the transverse unit vector defined as

$$\hat{\boldsymbol{t}} = \cos\delta\, \hat{\boldsymbol{i}}_T + \sin\delta\, \hat{\boldsymbol{i}}_N \tag{9}$$

and $a_r$ (or $a_t$) is the radial (or transverse) component of the propulsive acceleration given by

$$a_r = \frac{W_\oplus\, A_{\text{tot}}}{c\, m} \left(\frac{r_\oplus}{r}\right)^2 \widetilde{a}_r \tag{10}$$

$$a_t = \frac{W_\oplus\, A_{\text{tot}}}{c\, m} \left(\frac{r_\oplus}{r}\right)^2 \widetilde{a}_t \tag{11}$$

in which $\{\widetilde{a}_r, \widetilde{a}_t\}$ are dimensionless propulsive acceleration components defined as

$$\widetilde{a}_r = \cos\alpha\, (b_1 + b_2 \cos^2\alpha + b_3 \cos\alpha) \quad , \quad \widetilde{a}_t = \cos\alpha \sin\alpha\, (b_2 \cos\alpha + b_3) \tag{12}$$

*2.1. Sail force model in presence of EMPs*

The effect of the presence of EMPs on the solar sail thrust vector can be described through a simplified mathematical model [21]. To that end, the total sail reflective area $A_{\text{tot}}$ is assumed to consists of two parts, as is schematically shown in Fig. 2. The first part is constituted by a highly-reflective film of area $A_s$, with $A_s \leq A_{\text{tot}}$, while the rest of the exposed surface is covered by EMPs of (total) area $A_{\text{EMP}} = A_{\text{tot}} - A_s$. In particular, a part of the sail surface covered by electrochromic material, of area $A_{\text{EMP}}^{\text{on}} \leq A_{\text{EMP}}$, can be set

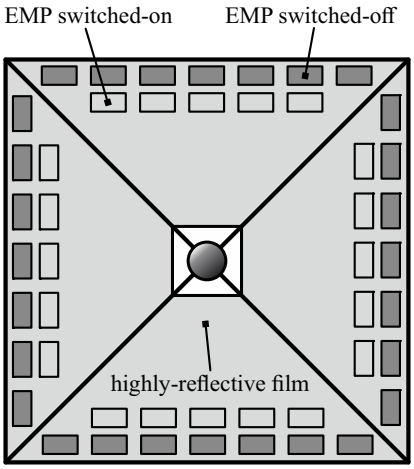


Figure 2: Schematic representation of a square solar sail with EMPs.

to a "high reflection mode" by switching the corresponding EMPs on, whereas the remaining part, of area $A_{\rm EMP}^{\rm off} = A_{\rm EMP} - A_{\rm EMP}^{\rm on}$, exhibits a diffuse reflection with $\rho = 1$, $s = 0$, and $B_f = 2/3$.

Assuming that the optical properties of the highly-reflective film coincide with those of the switched-on EMPs [21], a fraction

$$f = \frac{A_s + A_{\rm EMP}^{\rm on}}{A_{\rm tot}} \in [A_s/A_{\rm tot},\, 1] \tag{13}$$

of the total sail surface has force coefficients $\{b_1^{\rm on}, b_2^{\rm on}, b_3^{\rm on}\}$, while the remaining sail surface (that is, the part that exhibits the diffuse reflection) has force coefficients $\{b_1^{\rm off}, b_2^{\rm off}, b_3^{\rm off}\}$. Using the values of the optical parameters obtained in recent experimental tests [13] and bearing in mind Eqs. (3)–(5), the force coefficient of the highly-reflective sail surface of area $(A_s + A_{\rm EMP}^{\rm on}) \equiv f\, A_{\rm tot}$ are $b_1^{\rm on} \simeq 0.1901$, $b_2^{\rm on} \simeq 1.6198$, and $b_3^{\rm on} \simeq 0.0299$. On the other hand, the force coefficients of the sail surface of area $A_{\rm EMP}^{\rm off} \equiv (1-f)\, A_{\rm tot}$ are $b_1^{\rm off} = 1$, $b_2^{\rm off} = 0$, and $b_3^{\rm off} = 2/3$.

In presence of EMPs, the sail propulsive acceleration vector is again given by Eq. (2), but the generic force coefficient $b_i$, with $i = \{1, 2, 3\}$, is now written as

$$b_i = f\, b_i^{\rm on} + (1-f)\, b_i^{\rm off} \tag{14}$$

Taking into account Eqs. (12), the dimensionless components of the propulsive acceleration $\{\widetilde{a}_r,\, \widetilde{a}_t\}$ depend on two parameters $\{\alpha,\, f\}$, and the curve levels of the functions $\widetilde{a}_r = \widetilde{a}_r(\alpha, f)$ and $\widetilde{a}_t = \widetilde{a}_t(\alpha, f)$ are shown in Fig. 3. Note that the limiting case of $f = 1$ (or $f = 0$) refers to a solar sail in which the whole surface exhibits high (or diffuse) reflection. The case of $f = 1$ is obtained in a typical solar sail configuration without EMPs (that is, when $A_{\rm EMP} = 0$ and $A_s \equiv A_{\rm tot}$), or in a solar sail covered by switched-on EMPs (that is, when $A_{\rm EMP} = A_{\rm EMP}^{\rm on}$). On the other hand, the case of $f = 0$ is obtained when the whole solar sail is covered by switched-off EMPs, that is, when $A_s = 0$ and $A_{\rm EMP} = A_{\rm EMP}^{\rm off} = A_{\rm tot}$.

### *2.2. Trajectory control with TSI fluctuations*

Usually, solar sail-based orbit-to-orbit transfers are studied in an optimal framework by minimizing the total flight time [25, 10, 12]. During the preliminary mission design phase, the optimal transfer trajectory is calculated considering constant solar properties, that is, assuming a fixed value of parameter $W_\oplus$ in Eq. (2). In that case, the reference trajectory and the corresponding (reference) control law are simply the outputs of the optimization process.

However, due to the actual variability of the solar activity [9, 8], recent numerical simulations of heliocentric orbit transfers have shown that a solar sail-based spacecraft may substantially deviate from the reference trajectory when solar irradiance fluctuations (that is, fluctuations of the value of $W_\oplus$) are taken into account. In particular, the final position error with respect to a reference case of constant TSI is more pronounced when transfers with long flight times are considered [5]. A suitable control law is therefore

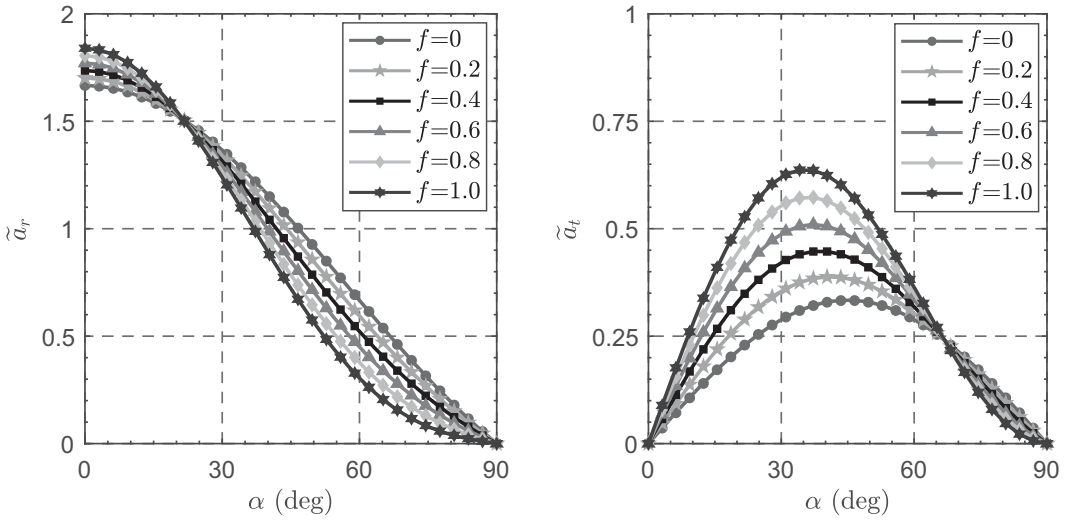


(a) Radial component.

(b) Transverse component.

Figure 3: Dimensionless components of propulsive acceleration as functions of $\alpha$ and $f$.

required to guarantee that the spacecraft may reach the target heliocentric orbit within prescribed tolerances. In the following discussion it is assumed that the spacecraft is able to estimate the actual value of $W_\oplus$ through the measurement of the local value $W$ of the TSI. The actual value of $W_\oplus$ is then obtained, at a generic Sun-spacecraft distance $r$, as [17]

$$W_\oplus = W \left(\frac{r}{r_\oplus}\right)^2 \tag{15}$$

The proposed control law allows the solar sail to track the optimal reference trajectory that is found under the assumption of a constant value $\overline{W}_\oplus \simeq 1360.8\,\mathrm{W/m^2}$ of TSI, and a constant value $\overline{f} = (A_s/A_{\mathrm{tot}} + 1)/2$ of the fraction $f$ defined in Eq. (13). In particular, $\overline{W}_\oplus$ coincides with the well known solar constant [16], and $\overline{f} \in [0.5,\, 1)$ is the mean value of the fraction $f$. Note that the fraction $f$ is excluded from the optimization variables when generating the reference trajectory. If, instead, $f$ were taken as a control variable to be optimized, it would result in a bang-bang type control. In that case a saturation problem could arise when considering the solar sail orbital motion with TSI fluctuations.

The reference control law $\{\alpha^{\mathrm{ref}},\, \delta^{\mathrm{ref}}\}$ is first obtained by solving the corresponding optimal control problem using an indirect approach [2, 18, 23], then Eqs. (12) and (14) give the corresponding (reference) time-variation of the dimensionless components of propulsive acceleration $\{\widetilde{a}_r^{\mathrm{ref}},\, \widetilde{a}_t^{\mathrm{ref}}\}$ as functions of $\alpha^{\mathrm{ref}}$ and $\overline{f}$, viz.

$$\begin{aligned}\widetilde{a}_r^{\mathrm{ref}} = {} & \overline{f}\, b_1^{\mathrm{on}} \cos\alpha^{\mathrm{ref}} + (1-\overline{f})\, b_1^{\mathrm{off}} \cos\alpha^{\mathrm{ref}} + \left[\overline{f}\, b_2^{\mathrm{on}} + (1-\overline{f})\, b_2^{\mathrm{off}}\right] \cos^3\alpha^{\mathrm{ref}} + \\ & + \left[\overline{f}\, b_3^{\mathrm{on}} + (1-\overline{f})\, b_3^{\mathrm{off}}\right] \cos^2\alpha^{\mathrm{ref}}\end{aligned} \tag{16}$$

$$\widetilde{a}_t^{\mathrm{ref}} = \cos\alpha^{\mathrm{ref}} \sin\alpha^{\mathrm{ref}} \left\{\left[\overline{f}\, b_2^{\mathrm{on}} + (1-\overline{f})\, b_2^{\mathrm{off}}\right] \cos\alpha^{\mathrm{ref}} + \left[\overline{f}\, b_3^{\mathrm{on}} + (1-\overline{f})\, b_3^{\mathrm{off}}\right]\right\} \tag{17}$$

Assuming that at each time instant the clock angle equals its reference value (i.e., $\delta = \delta^{\mathrm{ref}}$), the sail cone angle $\alpha$ and the fraction $f$ are adjusted in such a way that the radial and transverse components of propulsive acceleration fit their reference values $\{a_r^{\mathrm{ref}},\, a_t^{\mathrm{ref}}\}$ given by

$$a_r^{\mathrm{ref}} = \frac{\overline{W}_\oplus\, A_{\mathrm{tot}}}{c\, m} \left(\frac{r_\oplus}{r}\right)^2 \widetilde{a}_r^{\mathrm{ref}} \qquad , \qquad a_t^{\mathrm{ref}} = \frac{\overline{W}_\oplus\, A_{\mathrm{tot}}}{c\, m} \left(\frac{r_\oplus}{r}\right)^2 \widetilde{a}_t^{\mathrm{ref}} \tag{18}$$

Accordingly and bearing in mind Eqs. (10)-(11) and (18), the required values of $\alpha$ and $f$ are evaluated by enforcing the contraints

$$\widetilde{a}_r = \left(\overline{W}_\oplus / W_\oplus\right) \widetilde{a}_r^{\mathrm{ref}} \qquad , \qquad \widetilde{a}_t = \left(\overline{W}_\oplus / W_\oplus\right) \widetilde{a}_t^{\mathrm{ref}} \tag{19}$$

Taking into account the expressions of $\{\widetilde{a}_r,\, \widetilde{a}_t\}$ given by Eqs. (12), the required value of $f$ is obtained from Eqs. (19) as

$$f = \frac{\left(\overline{W}_\oplus / W_\oplus\right) \widetilde{a}_r^{\mathrm{ref}} - \left(b_1^{\mathrm{off}} \cos\alpha + b_2^{\mathrm{off}} \cos^3\alpha + b_3^{\mathrm{off}} \cos^2\alpha\right)}{\left(b_1^{\mathrm{on}} - b_1^{\mathrm{off}}\right) \cos\alpha + \left(b_2^{\mathrm{on}} - b_2^{\mathrm{off}}\right) \cos^3\alpha + \left(b_3^{\mathrm{on}} - b_3^{\mathrm{off}}\right) \cos^2\alpha} \tag{20}$$

in which the required sail cone angle $\alpha$ is obtained by solving the nonlinear equation

$$(K_1 - K_7) \cos\alpha \sin\alpha + K_2 \sin\alpha - K_3 - K_4 \cos^2\alpha - K_5 \cos\alpha - K_6 \cos^2\alpha \sin\alpha = 0 \tag{21}$$

where

$$\begin{gathered} K_1 = \left(\overline{W}_\oplus / W_\oplus\right) \widetilde{a}_r^{\mathrm{ref}} (b_2^{\mathrm{on}} - b_2^{\mathrm{off}}) \;,\; K_2 = \left(\overline{W}_\oplus / W_\oplus\right) \widetilde{a}_r^{\mathrm{ref}} (b_3^{\mathrm{on}} - b_3^{\mathrm{off}}) \;, \\ K_3 = \left(\overline{W}_\oplus / W_\oplus\right) \widetilde{a}_t^{\mathrm{ref}} (b_1^{\mathrm{on}} - b_1^{\mathrm{off}}) \;,\; K_4 = \left(\overline{W}_\oplus / W_\oplus\right) \widetilde{a}_t^{\mathrm{ref}} (b_2^{\mathrm{on}} - b_2^{\mathrm{off}}) \;, \\ K_5 = \left(\overline{W}_\oplus / W_\oplus\right) \widetilde{a}_t^{\mathrm{ref}} (b_3^{\mathrm{on}} - b_3^{\mathrm{off}}) \;,\; K_6 = b_1^{\mathrm{off}} b_2^{\mathrm{on}} - b_1^{\mathrm{on}} b_2^{\mathrm{off}} \;, K_7 = b_1^{\mathrm{off}} b_3^{\mathrm{on}} - b_1^{\mathrm{on}} b_3^{\mathrm{off}} \end{gathered} \tag{22}$$

Bearing in mind that $\alpha \in [0,\, 90]\,\mathrm{deg}$, Eq. (21) gives a sixth-order equation in $\cos\alpha$, viz.

$$\begin{gathered} -K_6^2 \cos^6\alpha + 2(K_1 - K_7) F \cos^5\alpha + \left[K_6^2 - (K_1 - K_7)^2 + 2K_2\, K_6 - K_4^2\right] \cos^4\alpha + \\ + \left[-2(K_1 - K_7)(K_2 + K_6) - 2K_4 K_5\right] \cos^3\alpha + \\ + \left[(K_1 - K_7)^2 - 2K_2\, K_6 - K_2^2 - K_5^2 - 2K_3\, K_4\right] \cos^2\alpha + \\ + \left[2K_2(K_1 - K_7) - 2K_3\, K_5\right] \cos\alpha + (K_2^2 - K_3^2) = 0 \end{gathered} \tag{23}$$

which may be solved numerically for $\alpha$ using standard algorithms. Then, the required fraction $f$ is obtained through Eq. (20). Note that when $\widetilde{a}_r^{\mathrm{ref}} = \widetilde{a}_t^{\mathrm{ref}} = 0$, the cone angle is $\alpha = 90\,\mathrm{deg}$ and the spacecraft tracks a Keplerian arc.

Because the short term fluctuations of $W_\oplus$ are usually very small [16, 5], the values of $\alpha$ and $f$ obtained as a solution of Eqs. (20) and (23) are close to the reference ones $\{\alpha^{\mathrm{ref}},\, \overline{f}\}$, as will be shown in the next section. In the event that Eq. (23) gives multiple solutions of $\alpha$, the value to be chosen is that as close as possible to the reference one, in order to avoid large sail attitude variations in short time-intervals. When, instead, no pair $\{\alpha,\, f\}$ exists that satisfies the enforced constraints, the spacecraft deviates from its nominal trajectory, and a rectification procedure is necessary. This case is similar to that discussed by [4]. However, the latter problem may be circumvented by slightly varying the reference value of the fraction $f$. In this sense, the proposed procedure allows the designer to choose a trade-off solution between transfer performance (in terms of flight time) and control law characteristics (in term of mean value of the fraction $f$).

### 3. Numerical simulations

The previously defined control law is now applied to a three-dimensional, orbit-to-orbit, Earth-Mars mission case assuming a low-performance solar sail with $m/A_{\mathrm{tot}} = 82.7\,\mathrm{g/m^2}$ and $\overline{f} = 0.9$. A solar sail with such values of $m/A_{\mathrm{tot}}$ and $\overline{f}$ has a characteristic acceleration $a_c = 0.1\,\mathrm{mm/s^2}$, the latter being defined as the maximum magnitude of the sail propulsive acceleration at a distance $r = r_\oplus$ from the Sun when the TSI is equal to $\overline{W}_\oplus$. In this example, the minimum flight time is about 3238 days, and the reference optimal transfer trajectory is shown in Fig. 4. Such a test case has been chosen due to the long transfer time it requires. Indeed, previous studies have shown that the error in the final position between a reference case of constant TSI and the case with variable TSI is larger for transfers with long flight times [5]. Therefore, in this case, the effectiveness of a control law that suitably counteracts the irradiance should be better appreciated.

According to the procedure described by [5], a value of $W_\oplus$ is randomly generated every 24 hours and a linear interpolation is used to evaluate the TSI over every one-day-long time interval. In this process, $W_\oplus$ is modelled as a Gaussian variable with a mean value

$$\mu_{W_\oplus} = W_\oplus^{\mathrm{min}} + \frac{\Delta W_\oplus}{2} \left[1 - \cos\left(\frac{2\,\pi\, t}{\Delta t_c}\right)\right] \tag{24}$$

and a standard deviation $\sigma_{W_\oplus} \simeq 2.35\,\mathrm{W/m^2}$, where $\Delta t_c = 11$ years, $W_\oplus^{\mathrm{min}} \simeq 1360.5\,\mathrm{W/m^2}$ is the TSI at the minimum solar activity, and $\Delta W_\oplus$ is the peak-to-peak amplitude (equal to the 0.1% of $\overline{W}_\oplus$) of the 11-year

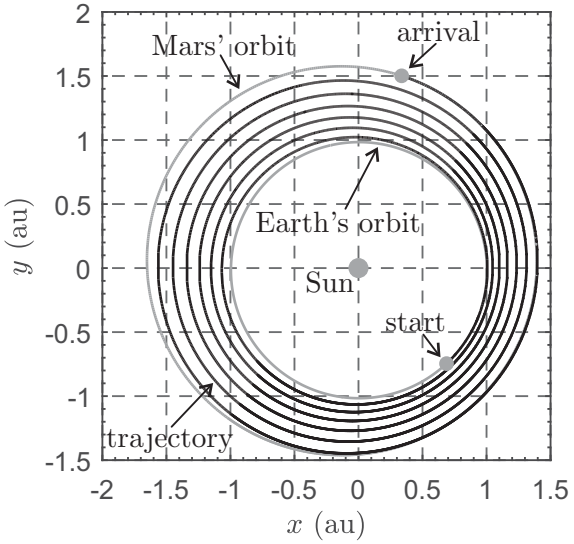


Figure 4: Ecliptic projection of the optimal reference Earth-Mars transfer trajectory with $\overline{f} = 0.9$ and $m/A_{\text{tot}} = 82.7\,\text{g/m}^2$.

solar cycle. A possible realization of TSI time history using this model is shown in Fig. 5, where the mean value variation of TSI in Eq. (24) is drawn with a solid line, whereas the grey points represent the values of TSI generated every 24 hours.

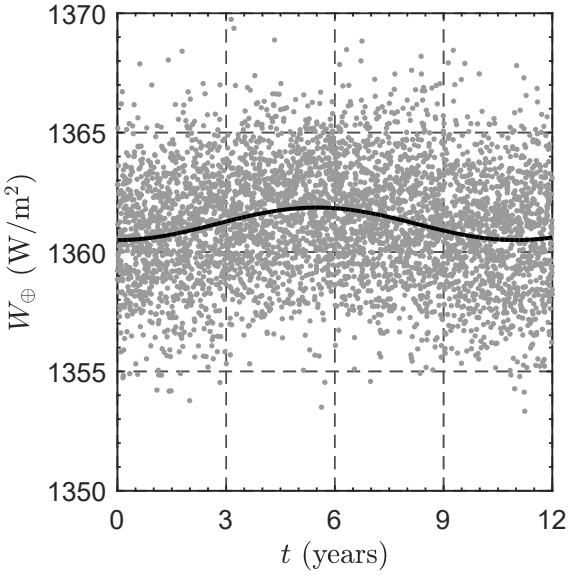


Figure 5: Variation of $\mu_{W_\oplus}$ due to the 11-year solar cycle (solid line), and a possible realization of TSI time history randomly generated according to the Gaussian distribution (grey dots).

Figures 6-7 show an example of the control law obtained with the proposed method. Similar results have been generated by other numerical simulations. The small oscillations of $\alpha$ (on the order of some tenths of degree in a few days) around its reference values can be observed in Fig. 6. Figure 7 shows that in this case $f$ never exceeds its boundary values, provided that at least the 12.5% of the total reflective surface is covered by EMPs.

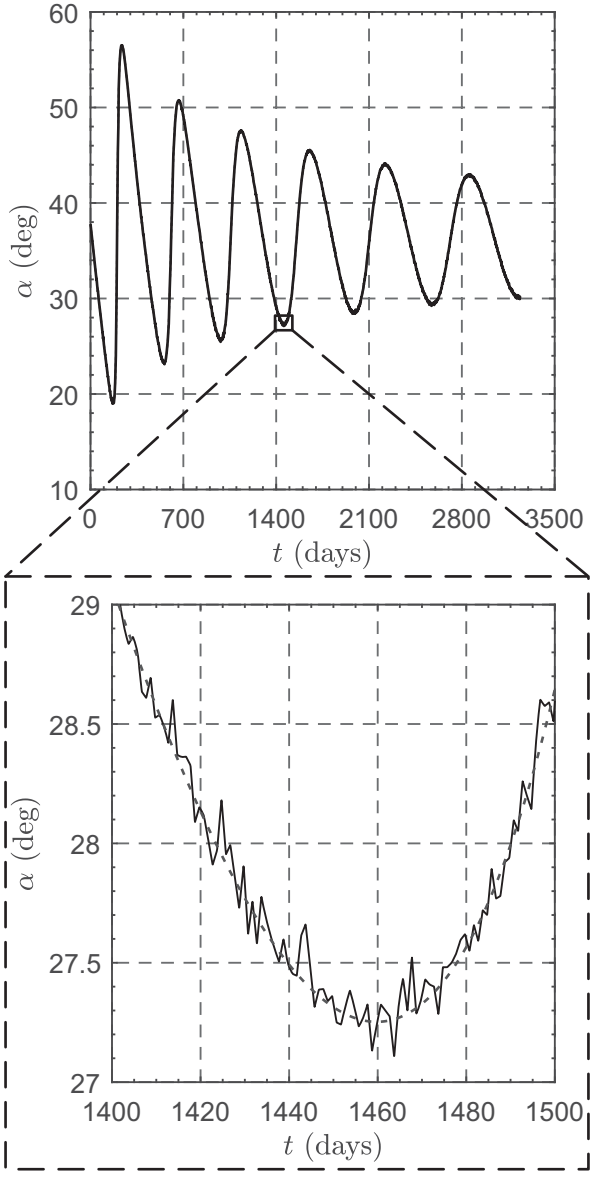


Figure 6: Optimal cone angle variation for an Earth-Mars transfer in the reference case (dotted line) and with fluctuations of TSI (solid line).

## 4. Conclusions

This work has proposed a possible control law aimed at counteracting the effects of solar irradiance fluctuations on the optimal heliocentric trajectory of a solar sail-based spacecraft. The sail surface is assumed to be made of a thin reflective film and partially covered by electrochromic material panels. The optimal solar sail transfer is essentially made of a reference trajectory, which corresponds to the case when the total solar irradiance is constant, and a compensation trajectory, which is introduced to model the actual short term fluctuations of the solar irradiance. The generation of the reference trajectory is a standard problem, which may be solved by suitably orienting the sail nominal plane. The compensation trajectory is instead obtained by varying the reflectivity of the electrochromic panels in such a way as to track the fluctuations of the solar irradiance. The proposed approach has been tested on a three-dimensional Earth-Mars transfer. The simulation results have shown that small variations of the control parameters are sufficient for the spacecraft to accurately track the reference heliocentric transfer trajectory. Finally, this work may be the

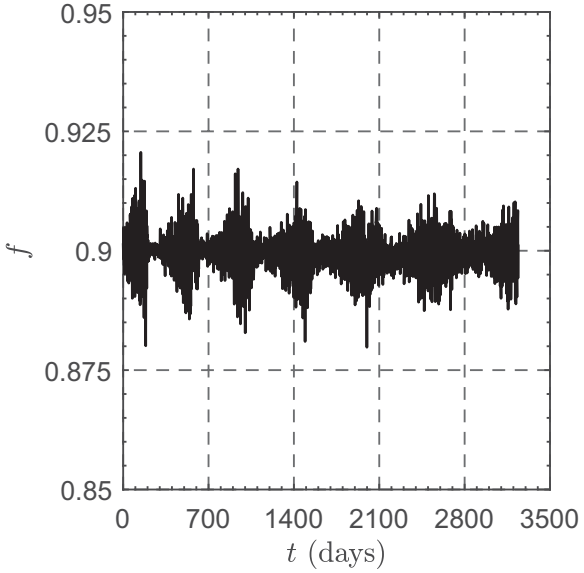


Figure 7: Required variation $f = f(t)$ for an Earth-Mars transfer assuming $\overline{f} = 0.9$.

basis of further research that may account for other uncertainty sources than solar irradiance fluctuation, such as orbital determination, control of execution errors, or the effects of environment and properties of the reflecting surface on the optical parameters of a solar sail.

## References


[1] Aliasi, G., Mengali, G., Quarta, A. A., Artificial lagrange points for solar sail with electrochromic material panels. Journal of Guidance, Control, and Dynamics 36 (5), 1544–1550, doi: 10.2514/1.58167, Sep. 2013.

[2] Bryson, A. E., Ho, Y. C., Applied Optimal Control. Hemisphere Publishing Corporation, New York, NY, Ch. 2, pp. 71–89, ISBN: 0-891-16228-3, 1975.

[3] Caruso, A., Bassetto, M., Mengali, G., Quarta, A. A., Optimal solar sail trajectory approximation with finite Fourier series. Advances in Space Research (in press), doi: 10.1016/j.asr.2019.11.019, 2020.

[4] Caruso, A., Niccolai, L., Mengali, G., Quarta, A. A., Electric sail trajectory correction in presence of environmental uncertainties. Aerospace Science and Technology 94 (paper n.105395), doi: 10.1016/j.ast.2019.105395, Nov. 2019.

[5] Caruso, A., Niccolai, L., Quarta, A. A., Mengali, G., Role of solar irradiance fluctuations on optimal solar sail trajectories. Journal of Spacecraft and Rockets (in press), doi: 10.2514/1.A34709, 2020.

[6] Caruso, A., Quarta, A. A., Mengali, G., Comparison between direct and indirect approach to solar sail circle-to-circle orbit raising optimization. Astrodynamics 3 (3), 273–284, doi: 10.1007/s42064-019-0040-x, Sep. 2019.

[7] Coddington, O., Lean, J., Pilewskie, P. e. a., Solar irradiance variability: Comparisons of models and measurements. Earth and Space Science 6 (12), 2525–2555, doi: 10.1029/2019EA000693, Dec. 2019.

[8] Fox, P., Solar Activity and Irradiance Variations. American Geophysical Union (AGU), pp. 141–170, ISBN: 9781118665909, 2013.

[9] Fröhlich, C., Lean, J., Solar radiative output and its variability: Evidence and mechanisms. Astronomy and Astrophysics Review 12 (4), 273–320, doi: 10.1007/s00159-004-0024-1, 2004.

[10] Fu, B., Sperber, E., Eke, F., Solar sail technology–a state of the art review. Progress in Aerospace Sciences 86, 1–19, doi: 10.1016/j.paerosci.2016.07.001, October 2016.

[11] Funase, R., Shirasawa, Y., Mimasu, Y., et al., On-orbit verification of fuel-free attitude control system for spinning solar sail utilizing solar radiation pressure. Advances in Space Research 48 (11), 1740–1746, doi: 10.1016/j.asr.2011.02.022, Dec. 2011.

[12] Gong, S., Macdonald, M., Review on solar sail technology. Astrodynamics 3 (2), 93–125, doi: 10.1007/s42064-019-0038-x, Jun. 2019.

[13] Heaton, A., Ahmed, N., Miller, K., Near earth asteroid Scout thrust and torque model. Presentation at 4th International Symposium on Solar Sailing (ISSS 2017), Kyoto, Japan, Jan. 2017.

[14] Hirai, T., Yano, H., Fujii, M., et al., Data screening and reduction in interplanetary dust measurement by IKAROS-ALADDIN. Advances in Space Research 59 (6), 1450–1459, doi: 10.1016/j.asr.2016.12.023, Mar. 2017.

[15] Hu, T., Gong, S., Mu, J., et al., Switch programming of reflectivity control devices for the coupled dynamics of a solar sail. Advances in Space Research 57 (5), 1147–1158, doi: 10.1016/j.asr.2015.12.029, Mar. 2016.

[16] Kopp, G., Lean, J. L., A new, lower value of total solar irradiance: Evidence and climate significance. Geophysical Research Letters 38 (1), 1–7, doi: 10.1029/2010GL045777, Jan. 2011.

[17] McInnes, C. R., Solar Sailing: Technology, Dynamics and Mission Applications. Springer-Verlag Berlin, Ch. 2, pp. 47–51, ISBN: 978-1-85233-102-3, 1999.
[18] Mengali, G., Quarta, A. A., Optimal three-dimensional interplanetary rendezvous using nonideal solar sail. Journal of Guidance, Control, and Dynamics 28 (1), 173–177, doi: 10.2514/1.8325, January-February 2005.
[19] Mengali, G., Quarta, A. A., Heliocentric trajectory analysis of sun-pointing smart dust with electrochromic control. Advances in Space Research 57 (4), 991–1001, doi: 10.1016/j.asr.2015.12.017, Feb. 2016.
[20] Monk, P. M. S., Mortimer, R. J., Rosseinsky, D. R., Electrochromism: Fundamentals and Applications. John Wiley & Son, pp. 57–58, Jun. 1995.
[21] Mu, J., Gong, S., Li, J., Coupled control of reflectivity modulated solar sail for geosail formation flying. Journal of Guidance, Control, and Dynamics 38 (4), 740–751, doi: 10.2514/1.G000117, Apr. 2015.
[22] Niccolai, L., Bassetto, M., Quarta, A. A., Mengali, G., A review of smart dust architecture, dynamics, and mission applications. Progress in Aerospace Sciences 106, 1–14, doi: 10.1016/j.paerosci.2019.01.003, Apr. 2019.
[23] Niccolai, L., Quarta, A. A., Mengali, G., Analytical solution of the optimal steering law for non-ideal solar sail. Aerospace Science and Technology 62, 11–18, doi: 10.1016/j.ast.2016.11.031, March 2017.
[24] Pap, J. M., Fröhlich, C., Total solar irradiance variations. Journal of Atmospheric and Solar-Terrestrial Physics 61 (1-2), 15–24, doi: 10.1016/S1364-6826(98)00112-6, Jan. 1999.
[25] Sauer, C. G., Optimum solar-sail interplanetary trajectories. Presentation at AIAA/AAS Astrodynamics Conference, San Diego, California, Aug. 1976.
[26] Vulpetti, G., Effect of the total solar irradiance variations on solar-sail low-eccentricity orbits. Acta Astronautica 67 (1-2), 279–283, doi: 10.1016/j.actaastro.2010.02.004, Jul. 2010.
[27] Vulpetti, G., Total solar irradiance fluctuation effects on sailcraft-Mars rendezvous. Acta Astronautica 68 (5-6), 644–650, doi: 10.1016/j.actaastro.2010.01.010, Mar. 2011.
[28] Vulpetti, G., Fast Solar Sailing - Astrodynamics of Special Sailcraft Trajectories. Space Technology Library. Springer Netherlands, Ch. 3, p. 89, 2013.
[29] Zola, D., Circi, C., Vulpetti, G., Scaglione, S., Photon momentum change of quasi-smooth solar sails. Journal of the Optical Society of America A: Optics and Image Science, and Vision 35 (8), 1261–1271, doi: 10.1364/JOSAA.35.001261, Aug. 2018.